RESEARCH ARTICLE

WILEY

D-pinitol alleviates diabetic cardiomyopathy by inhibiting the optineurin-mediated endoplasmic reticulum stress and glycophagy signaling pathway

Xiaoli Li[1] | Xin Yu[2,3,4] | Fei Yu[2,3,4] | Chunli Fu[2,3,4] | Wenqian Zhao[2,3,4] | Xiaosong Liu[2,3,4] | Chaochao Dai[2,3,4] | Haiqing Gao[2,3,4] | Mei Cheng[2,3,4] | Baoying Li[3,5] (iD)

[1]Department of Pharmacy, Qilu Hospital of Shandong University, Jinan, China

[2]Department of Geriatric Medicine, Qilu Hospital of Shandong University, Jinan, China

[3]Key Laboratory of Cardiovascular Proteomics of Shandong Province, Qilu Hospital of Shandong University, Jinan, China

[4]Jinan Clinical Research Center for Geriatric Medicine (202132001), Jinan, China

[5]Health Management Center (East Area), Qilu Hospital of Shandong University, Jinan, China

Correspondence
Baoying Li and Mei Cheng, Key Laboratory of Cardiovascular Proteomics of Shandong Province, Qilu Hospital of Shandong University, 107 Wenhuaxi Road, Jinan, Shandong Province 250012, People's Republic of China.
Email: libaoying77@163.com; jncm65@email.sdu.edu.cn

Abstract

Diabetic cardiomyopathy (DCM) is an important complication resulting in heart failure and death of diabetic patients. However, there is no effective drug for treatments. This study investigated the effect of D-pinitol (DP) on cardiac injury using diabetic mice and glycosylation injury of cardiomyocytes and its molecular mechanisms. We established the streptozotocin-induced SAMR1 and SAMP8 mice and DP (150 mg/kg/day) intragastrically and advanced glycation end-products (AGEs)-induced H9C2 cells. H9C2 cells were transfected with optineurin (OPTN) siRNA and overexpression plasmids. The metabolic disorder indices, cardiac dysfunction, histopathology, immunofluorescence, western blot, and immunoprecipitation were investigated. Our results showed that DP reduced the blood glucose and AGEs, and increased the expression of heart OPTN in diabetic mice and H9C2 cells, thereby inhibiting the endoplasmic reticulum stress (GRP78, CHOP) and glycophagy (STBD1, GABARAPL1), and alleviating the myocardial apoptosis and fibrosis of DCM. The expression of filamin A as an interaction protein of OPTN downregulated by AGEs decreased OPTN abundance. Moreover, OPTN siRNA increased the expression of GRP78, CHOP, STBD1, and GABARAPL1 and inhibited the expression of GAA via GSK3β phosphorylation and FoxO1. DP may be helpful to treat the onset of DCM. Targeting OPTN with DP could be translated into clinical application in the fighting against DCM.

KEYWORDS
diabetic cardiomyopathy, D-pinitol, endoplasmic reticulum stress, glycophagy, optineurin

1 | INTRODUCTION

Diabetic cardiomyopathy (DCM) is a pathophysiological condition that results in heart failure in diabetic patients and increases mortality throughout the world and the burden of economic and social. The pathophysiological mechanisms of DCM include advanced glycation end-products (AGEs), deposition, oxidative stress, endoplasmic reticulum stress (ERS), glycophagy dysregulation, mitochondrial dysfunction, increased myocyte apoptosis and fibrosis, etc (Jia et al., 2016, 2018; Zhao et al., 2018). However, the relationship between ERS and glycophagy has not been fully unraveled.

ERS plays a crucial role in the development of myocardial apoptosis and fibrosis in DCM. Endoplasmic reticulum is a complex intracellular membrane network, which regulates protein folding and

modification (Li, Yu, et al., 2022; Li, Zhang, et al., 2022). A variety of factors including hyperglycemia, AGEs accumulation, oxidative stress, and ischemia, cause the accumulation of unfolded proteins, and trigger unfolded protein response, which ultimately leads to myocardial apoptosis and hypertrophy (Fernández et al., 2015; He et al., 2018). Glucose-regulated protein 78 (GRP78) and C/EBP homologous protein (CHOP) as markers of ERS play an important role in DCM (Preetha Rani et al., 2022). Moreover, ERS can induce autophagy, and autophagy protects ERS-mediated apoptosis by negative feedback. The crosstalk between ERS and autophagy indicates that ERS is involved in autophagic events (Mandl & Bánhegyi, 2018). On the contrary, excessive autophagy can also lead to atherosclerosis and cell death. Glycophagy is a special type of autophagy that is crucial for regulating glycogen catabolism. It is a double-edged sword that can provide both endogenous protection and endogenous damage. The expression of gamma-aminobutyric acid receptor-associated protein-like 1 (GABARAPL1) and starch binding domain-containing protein 1 (STBD1), as glycophagy markers, was increased in the heart of streptozotocin (STZ)-induced diabetic rats (Mellor et al., 2014). Acid alpha-glucosidase (GAA) plays an important role in lysosomal glycogenolysis. Many studies have reported that glycophagy aggravates the myocardial injury of diabetes and ultimately leads to the onset and development of DCM (Koutsifeli et al., 2022; Zhao et al., 2018).

Optineurin (OPTN) is an autophagic receptor that participates in many crucial cellular processes such as cell division, autophagy, transportation of protein, and membrane cargo (Hu et al., 2023; Qiu et al., 2022). Chen et al. reported that high glucose significantly inhibited the levels of OPTN mRNA and protein in murine renal tubular epithelial cells. OPTN inhibited the activation of NOD-like receptor thermal protein domain-associated protein 3 inflammasomes and reduced the level of mitochondrial reactive oxygen species in diabetic nephropathy (Chen et al., 2019). Moreover, it is found that OPTN knockdown was related to activation ERS response and chaperones-mediated autophagy in the pancreatic ductal adenocarcinoma cells (Ali et al., 2019). Therefore, it is of great clinical significance to elucidate the molecular mechanism OPTN-modulated ERS and glycophagy in DCM, and to search for effective drug targets for treatment.

Our previous research found that D-pinitol (methyl ether of D-chiro-inositol, DP) could inhibit the myocardial apoptosis and fibrosis in STZ-induced senescence-accelerated prone 8 (SAMP8) mice. The protective effect of DP on DCM was related to the regulation of OPTN (Li et al., 2021; Li, Yu, et al., 2022; Li, Zhang, et al., 2022). DP is found in large quantities in soybean, carob pods, and legume foods. DP has been pharmacologically evaluated for its antidiabetic, antioxidant, antiageing, cardioprotective, renoprotective, and anticancer efficacies (Liu et al., 2022; Medina-Vera et al., 2022). Oral DP can be easily absorbed and cleared, and plays an insulin-like role and directly activates insulin signaling processes in diabetic animal models. However, the molecular mechanism of DP in treating DCM has not been elucidated.

The objective of the present study was to investigate the effect of DP on DCM using the STZ-induced SAMR1 and SAMP8 mice and AGEs-induced H9C2 cells. The molecular mechanism of DP and OPTN-modulated ERS and glycophagy was evaluated in the experiment.

2 | MATERIALS AND METHODS

2.1 | Materials

D-pinitol (Lot No: BCCB9551, purity 95%) and STZ were purchased from Sigma Aldrich (St. Louis, USA). AGEs was purchased from Bioss Biotechnology Co., Ltd (Beijing, China). Bovine serum albumin (BSA) was purchased from Meilunbio (Dalian, China). The antibodies of OPTN (10837-1-AP), GABARAPL1 (11010-1-AP), GRP78 (11587-1-AP), CHOP (15204-1-AP), glycogen synthase kinase-3β (GSK3β, 22,104-1-AP), p-GSK3β (Ser9, 67,558-1-Ig), GAA (14367-1-AP), and β-actin (20536-1-AP) were all purchased from Proteintech (Wuhan, China). The antibody of filamin A (FLNA, sc-17,749) was purchased from Santa Cruz Biotechnology (Dallas, USA). The antibodies of GAA (A19234) and forkhead box O1 (FoxO1, A2934) were purchased from ABclonal (Wuhan, China). The antibody of STBD1 (Df12326) was purchased from Affinity Biosciences (Changzhou, China). The antibody of FLNA (BM4039) was purchased from BOSTER (Wuhan, China). The cell counting kit-8 (CCK-8) was purchased from MedChem Express (New Jersey, USA). IP/CO-IP extraction kit was purchased from Abbkine Scientific (Wuhan, China). The mouse AGEs ELISA kit was purchased from Jiyinmei Biotechnology (Wuhan, China). Lipofectamine 3000 was purchased from Thermo Fisher Scientific (Waltham, USA). Annexin V-FITC/PI cell apoptosis detection kit was purchased from Bergolin (Dalian, China). Glycogen content and reactive oxygen species (ROS) assay kit were purchased from Solarbio (Beijing, China). All other chemical reagents were purchased with analytical grade.

2.2 | Animals and groups

Detailed methods were described in Supplementary Material. CCR (n = 10): control SAMR1 group, DMR (n = 13): STZ-induced SAMR1 group, CCP (n = 10): control SAMP8 group, DMP (n = 13): STZ-induced SAMP8 group, DDP (n = 13): DP-treated STZ-induced SAMP8 group. All procedures were approved by the Animal Ethics Committee of Shandong University (Approval No: 21170). All animal experiments were carried out according to the Laboratory Animal Center's guidelines of Shandong University in compliance with the ARRIVE guidelines.

2.3 | Echocardiography

Before the end of the experiments, transthoracic echocardiographic images of hearts were obtained by Vevo 770 machine equipped with a 30-MHz transducer (VisualSonics, Toronto, ON, Canada) under isoflurane anesthesia.

2.4 | Determination of body weight (BW), heart weight (HW)/BW, fasting blood glucose (FBG), AGEs, and heart glycogen

Animals were weighed every week. At the end of the study, the HW was measured and calculated the ratios of HW/BW (mg/g). Serum FBG was determined by DVI-1650 Automatic Biochemistry and Analysis Instrument (Bayer, Germany). Serum and cardiac AGEs, and cardiac glycogen contents were determined according to the manufacturer's instructions.

2.5 | Light microscopy

Hearts were excised and fixed in 4% paraformaldehyde, embedded in paraffin, and cut into 4-μm-thick sections. Then, they were stained with hematoxylin and eosin (HE), Masson's Trichrome, Periodic Acid-Schiff (PAS), immunofluorescence (OPTN 1:200), and immunohistochemistry (STBD1, GRP78, GAA 1:200).

2.6 | Transmission electron microscope

The hearts were cut into cubes of 1 mm^3 in size, immediately put into the transmission electron microscope (TEM) fixative, and then embedded with resin. The slices were obtained using Leica UC7 microsystems, then stained by uranium acetate-saturated alcohol and lead citrate. The ultrathin sections were examined with an HT7800 TEM (Hitachi, Japan).

2.7 | Cell cultures

H9C2 cells (rat heart myoblast cell line) were obtained from the Shanghai QiDa Biotechnology (Shanghai, China). H9C2 cells were cultured in DMEM medium containing 10% FBS in an incubator with a volume fraction of 5% CO_2 at 37°C. Logarithmic growth cells in good condition were used for the following experiments.

2.8 | Knockdown of OPTN by small interfering RNAs (siRNA) and overexpression plasmid transfection

OPTN siRNAs and negative control siRNAs were designed and chemically synthesized from Shanghai GenePharma (Shanghai, China). The siRNA sequence targeting OPTN included: sense 5′-GCCAGUU-GUUUGAGAUACATT-3′, antisense 5′-UGUAUCUCAAACAAC UGGCTT-3′. The sequence of negative control siRNA is: sense 5′-UUCUCCGAA CGUGUCACGUTT-3′, antisense 5′-ACGUGACAC-GUUCGGAGAATT-3′. The overexpression plasmids Rattus-OPTN (GenBank accession no: NM_145081.4) were constructed by Shanghai BioSune Biotechnology (Shanghai, China). H9C2 cells were transfected with OPTN siRNA and overexpression plasmids using Lipofectamine 3000 according to the manufacturer's instructions. The OPTN expression was measured by real-time polymerase chain reaction (RT-PCR) and western blot at 24, 48 h after transfection.

2.9 | Co-immunoprecipitation (CO-IP)

H9C2 cells with overexpressing OPTN were lysed using the CO-IP extraction kit. The lysates were incubated with either anti-OPTN antibody or IgG overnight at 4°C. Then, the beads were boiled in an SDS loading buffer for CO-IP assay and western blot validation. The interacting proteins of OPTN were identified with Q-Exactive HF LC–MS/MS (Thermo Fisher Scientific, USA). Detailed methods and database searching were described in Supplementary Material.

2.10 | Immunofluorescence

H9C2 cells were fixed with 4% paraformaldehyde for 15 min and were permeabilized with 0.5% Triton X-100 for 20 min from the various treatment groups. After blocking with 5% BSA for 30 min, the cells were incubated with primary antibodies (OPTN, STBD1, GRP78, FLNA 1:100) at 4°C overnight. Subsequently, the cells were incubated with fluorescence staining secondary antibody for 60 min at room temperature. Cell fluorescence was observed by a fluorescence microscope (Olympus BX53, Japan) and was evaluated by Fiji Image software. The results were expressed as mean fluorescence intensity (MFI).

2.11 | Western blot analysis

The heart and H9C2 cells samples were homogenized in ice-cold lysis buffer containing PMSF (Beyotime Biotechnology, Jiangsu, China). An equal amount of protein was separated by SDS-PAGE (10%) and transferred onto polyvinylidene difluoride membranes. The membrane was sealed with PBST-5% skimmed milk or PBST-5% BSA and then incubated overnight with the antibody at 4°C as follows: OPTN (1:5000), STBD1 (1:1000), GABARAPL1 (1:1000), GRP78 (1:5000), CHOP (1:1000), GAA (1:1000), FLNA (1:1000), GSK3β (1:5000), pho-GSK3β (Ser9, 1:1000), and FoxO1 (1:1000). Secondary antibody (Beyotime, China) was applied for 1 h at room temperature. The intensity of immunoblot bands was normalized to that of β-actin (1:2000). Densitometry was obtained for quantification of each identified protein band and analyzed with Image J densitometry software.

2.12 | Statistical analysis

Data were expressed as mean ± standard deviation. Statistical analysis between groups was made using one-way analysis of variance (ANOVA) followed by Tukey's post hoc test for multiple comparisons. p-value <0.05 was considered statistically significant. All analyses were performed with SPSS for Windows software version 22.0 (SPSS, Chicago, USA).

3 | RESULTS

3.1 | Effects of DP on BW, HW/BW, serum FBG and AGEs, cardiac AGEs and glycogen, and cardiac function

The mice number was 10, 10, 10, 10, and 11, respectively, of group CCR, DMR, CCP, DMP, and DDP at the end of experiment. The BW of diabetic groups (DMR and DMP) decreased significantly compared with the control group (CCR and CCP) at 23 weeks ($p < 0.01$). DP significantly increased the weight of diabetic mice (Figure 1a, $p < 0.01$). The ratios of HW/BW, serum FBG and AGEs concentrations, cardiac AGEs, and glycogen contents of the diabetic groups (DMR and DMP) were significantly higher than those of the control group (CCR and CCP), while those in the DDP group were decreased ($p < 0.01$) (Figure 1b–f).

Moreover, the cardiac function in left ventricular internal dimension diastole (LVIDd, mm) of mice was significantly increased, and the left ventricular volume in diastole (LVVd, μL), left ventricular ejection fractions (LVEF, %), fractional shortening (FS, %), and the ratio E peak/A peak (E/A) in the diabetic group were significantly reduced compared with that in the control group. However, after 8-week DP administration, the cardiac dysfunction was significantly improved in the diabetic mice (Figure 1g–l, $p < 0.01$).

3.2 | Effects of DP on cardiac histological findings and ultrastructure

Under light microscopy, the heart of diabetic groups (DMR and DMP) showed irregular arrangement of muscle fibers, edema, inflammatory cell infiltration, and extracellular matrix accumulation. Moreover, the cardiac fibrosis, collagen, and glycogen contents were significantly higher observed in the diabetic group (DMR and DMP) than those of control group (CCR and CCP). A decreased level of myocardial injury, fibrotic formation, and glycogen content were observed in the heart of DDP group when treated with DP (Figure 2a–c).

TEM analysis showed cardiomyocyte architecture in the hearts. The cardiomyocyte of diabetic group (DMR and DMP) showed sarcomeres and myofilament arrangements disturbance, sarcoplasmic reticulum dilation, glycogen particle aggregation, glycogen autophagosome and damaged mitochondria, and cristae appearing disordered. DP could significantly improve the subcellular structural damage in diabetic mice (Figure 2d).

3.3 | Effects of DP on OPTN, STBD1, GABARAPL1, GRP78, CHOP, and GAA in the heart of diabetic mice

By immunofluorescence, OPTN-positive expression was decreased in the heart tissues of diabetic groups (DMR and DMP), and DP significantly restored the OPTN-positive expression in the heart tissues (Figure 3a). MFI of OPTN was determined in the heart tissues (Figure 3b). By immunohistochemistry, STBD1 and GRP78-positive areas were increased, GAA-positive areas were decreased in the heart tissues of diabetic groups (DMR and DMP), while DP improved the STBD1, GRP78, and GAA-positive areas (Figure 3c). To further investigate the effect of DP on glycophagy and ERS, we measured the protein expression of OPTN, STBD1, GABARAPL1, GRP78, CHOP, and GAA by western blot. Consistently, DP increased the protein expression of OPTN and GAA, and inhibited the protein expression of STBD1, GABARAPL1, GRP78, and CHOP in the DDP group (Figure 3d–k, $p < 0.05$).

3.4 | Transduction efficiency and effects of OPTN on cell viability in H9C2 treated by AGEs

H9C2 carrying OPTN siRNA (OsiRNA) and negative control siRNA (NC), and EGFP (GFP) and OPTN overexpression plasmids (Oover) were harvested. The transduction efficiency was assessed by RT-PCR and western blot. The mRNA and protein expression of OPTN reached optimal transduction efficiency at 48 h (Supplementary Figures S1).

The structure of DP was shown in Supplementary Figure S2A. The cell viability of H9C2 cells was decreased in exposure to AGEs (0, 25.00, 50.00, 100.00, 200, 400 μg/mL) for 48 h (Supplementary Figure S2B). The cell viability was increased when H9C2 cells were exposed to DP at a concentration of ≤80.00 umol/L for 48 h (Supplementary Figure S2C). The DMSO, unmodified BSA, negative control siRNA, or GFP did not affect cell viability. Different concentrations of DP pretreatment (20, 40, 80 μmol/L) significantly improved the decrease of cell viability induced by AGEs (200 μg/mL) stimulation (Supplementary Figure S2D, $p < 0.01$). Moreover, OPTN siRNA significantly decreased cell viability ($p < 0.01$). The cell viability was increased when the OsiRNA group was exposed to DP for 48 h. OPTN overexpression significantly attenuated AGEs induced the decrease of cell viability compared with the GFP + AGEs group (Supplementary Figure S2E, $p < 0.01$) for 48 h.

3.5 | Effects of DP on ROS and OPTN on apoptosis in H9C2 treated by AGEs

The ROS formation was significantly increased by AGEs (200 μg/mL) stimulation, whereas pretreatment of DP (80 μmol/L) prevented AGEs-induced ROS generation for 48 h (Supplementary Figure S3A and S3B, $p < 0.01$).

The percentage of apoptotic cells was significantly increased by AGEs (200 μg/mL) stimulation for 48 h ($p < 0.01$). Pretreatment of H9C2 with DP (80 μmol/L) significantly improved the AGEs-stimulated cell apoptosis ($p < 0.01$). OPTN siRNA significantly increased the cell apoptosis ($p < 0.01$), while DP (80 μmol/L)
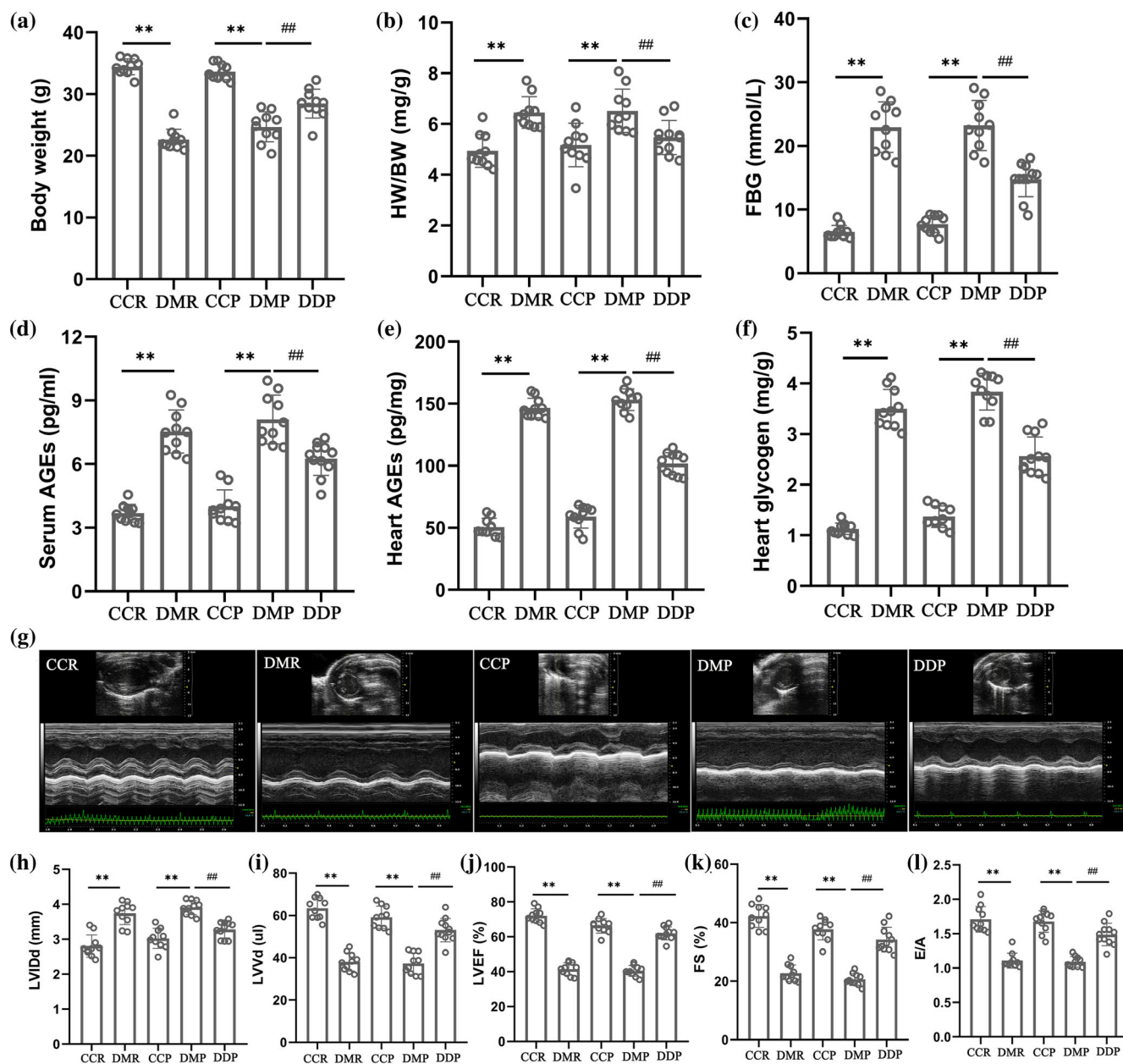
FIGURE 1 Effects of DP on BW, HW/BW, serum FBG and AGEs, cardiac AGEs and glycogen, and cardiac function in STZ-induced SAMP8. (a) Body weight changes of the mice. (b) HW/BW changes of the mice. (c) Serum FBG changes of the mice. (d) Serum AGEs changes of the mice. (e) Cardiac AGEs changes of the mice. (f) Cardiac glycogen changes of the mice. (g) Representative echocardiographic images of LV M-model in the mice. (h) Measurement of the LVIDd (mm) in the mice. (i) Measurement of the LVVd (mm) in the mice. (j) Measurement of LVEF (%) in the mice. (k) Measurement of FS (%) in the mice. (l) Measurement of the ratio E peak/A peak (E/A) in the mice. (A-L: CCR, $n = 10$; DMR, $n = 10$; CCP, $n = 10$; DMP, $n = 10$; DDP, $n = 11$). *$p < 0.05$, **$p < 0.01$ compared with control group (CCR and CCP); #$p < 0.05$, ##$p < 0.01$ compared with DMP group. CCR: control SAMR1 group; DMR: STZ-induced SAMR1 group; CCP: control SAMP8 group; DMP: STZ-induced SAMP8 group; DDP: DP-treated STZ-induced SAMP8 group. DP: D-pinitol; BW: body weight; HW/BW: heart weight/body weight; FBG: fasting blood glucose; AGEs: advanced glycation end-products; STZ: streptozotocin; LVIDd: left ventricular internal dimension diastole; LVVd: left ventricular volume in diastole; LVEF: left ventricular ejection fractions; FS: fractional shortening.

attenuated the cell apoptosis for 48 h. Induction of the GFP group with AGEs (200 μg/mL) resulted in a significant increase in cell apoptosis, whereas OPTN overexpression significantly attenuated AGEs-induced cell apoptosis for 48 h (Supplementary Figure S4A and S4B, $p < 0.01$).

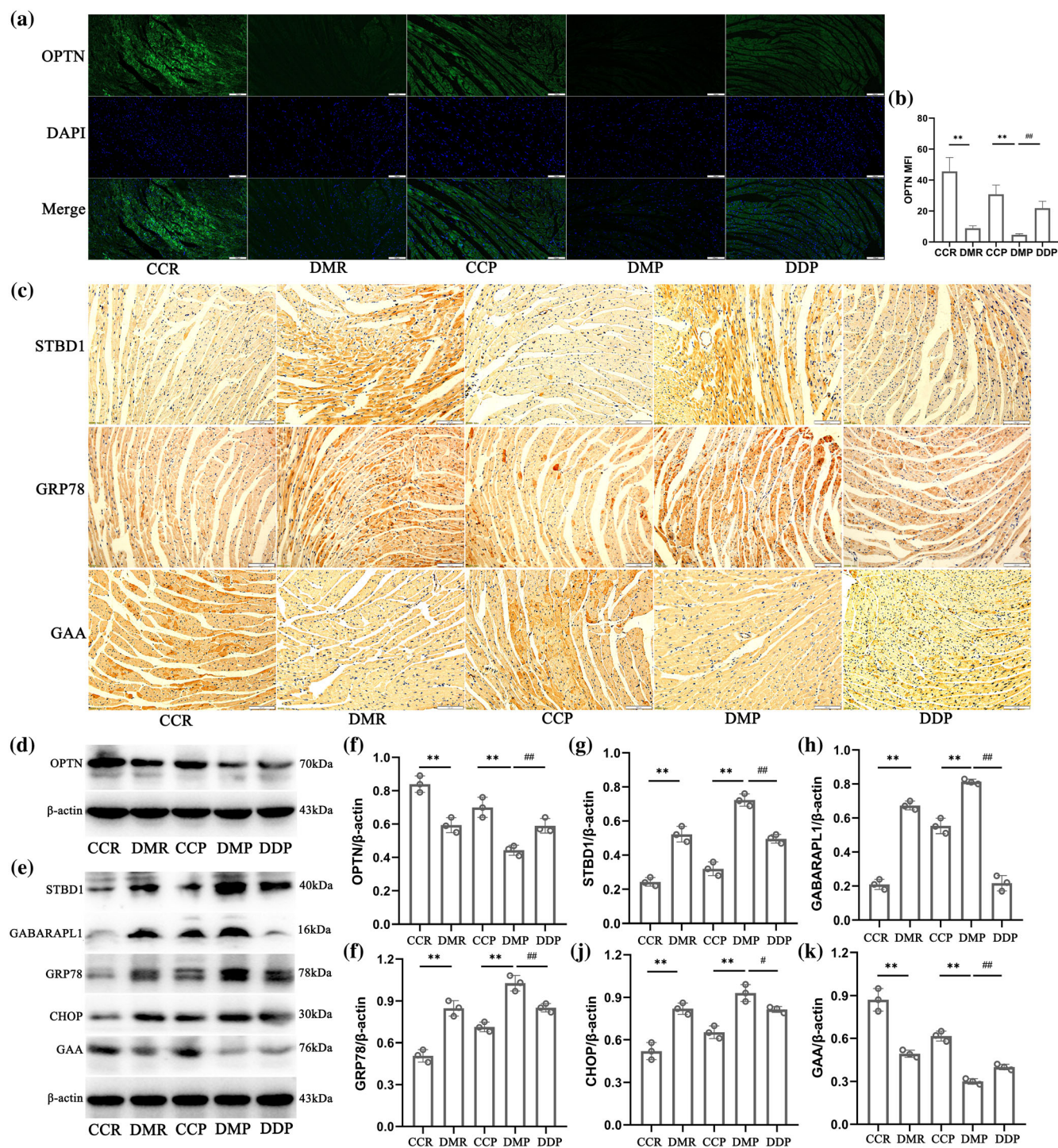## 3.6 | Effects of OPTN on STBD1, GABARAPL1, GRP78, CHOP, and GAA in H9C2 cells

The expression of OPTN, STBD1, and GRP78 was detected in H9C2 cells by immunofluorescence. Compared with CC group, the
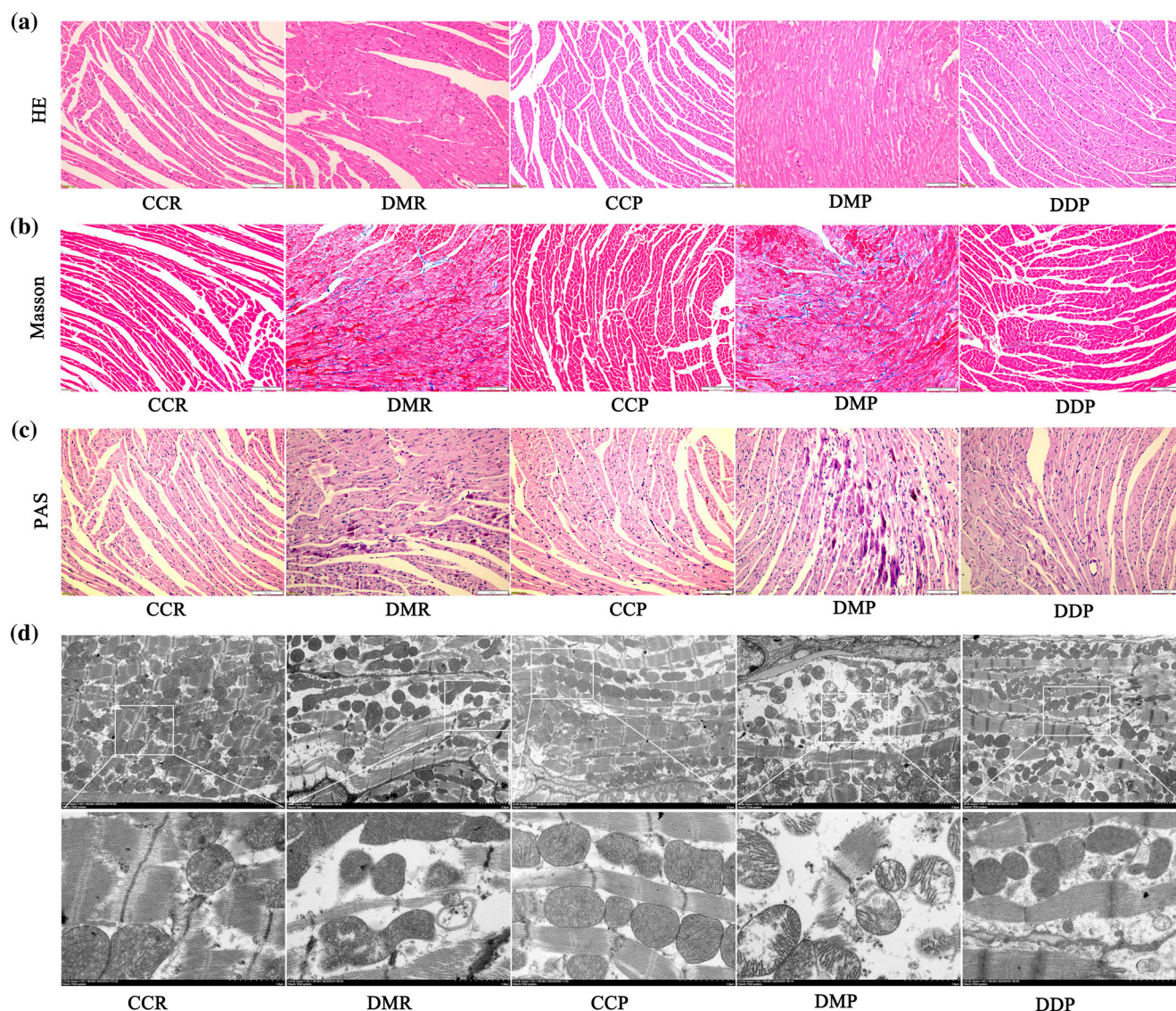
FIGURE 2 Effects of DP on cardiac histological findings and ultrastructure. (a) Representative light micrographs of the heart (HE, bar: 100 μm, $n = 5$). (b) Representative light micrographs of the heart (Masson's Trichrome, bar: 100 μm, $n = 5$). (c) Representative light micrographs of the heart (PAS, bar: 100 μm, $n = 5$). D: Transmission electron microscope images of the myocardium (bar: 2.0 μm, 1.0 um, $n = 5$). CCR: control SAMR1 group; DMR: STZ-induced SAMR1 group; CCP: control SAMP8 group; DMP: STZ-induced SAMP8 group; DDP: DP-treated STZ-induced SAMP8 group. DP: D-pinitol.

expression of OPTN was significantly decreased, and the expression of STBD1 and GRP78 was significantly increased in the AGEs group. Pretreatment of H9C2 with DP (80 μmol/L) significantly improved the expression of OPTN, STBD1, and GRP78 by AGEs (200 μg/mL) stimulation for 48 h. Induction of the CC group with AGEs (200 μg/mL) resulted in a significant increase in the expression of STBD1 and GRP78, whereas OPTN overexpression significantly attenuated AGEs induced the expression of STBD1 and GRP78 for 48 h. OPTN siRNA significantly increased the expression of STBD1 and GRP78 for 48 h (Figure 4a,b). MFI of OPTN, STBD1, and GRP78 was determined in H9C2 cells (Figure 4c–e). To further investigate the effect of OPTN and DP on glycophagy and ERS, we measured the protein expression of OPTN, STBD1, GABARAPL1, GRP78, CHOP, and GAA by western

blot. Consistently, DP increased the protein expression of OPTN and GAA and inhibited the protein expression of STBD1, GABARAPL1, GRP78, and CHOP in the DDP group (Figure 4f–h, $p < 0.05$). Stimulation of GFP group with AGEs (200 μg/mL) resulted in a significant increase in the protein expression of STBD1, GABARAPL1, GRP78, and CHOP, and a significant decrease in the protein expression of GAA, whereas OPTN overexpression significantly attenuated AGEs induced the protein expression of STBD1, GABARAPL1, GRP78, CHOP, and GAA compared with GFP + AGEs group (Figure 4i–k, $p < 0.05$). Moreover, the protein expression of STBD1, GABARAPL1, GRP78, and CHOP significantly increased, the protein expression of GAA significantly decreased in OsiRNA group compared with those in NC group (Figure 4l–n, $p < 0.01$). But both OsiRNA+DP group and

FIGURE 3 Effects of DP on OPTN, STBD1, GABARAPL1, GRP78, CHOP, and GAA in the heart of diabetic mice. (a) Immunofluorescent images of OPTN in the heart tissues (bar: 100 μm, $N = 5$). (b) MFI of OPTN in the heart tissues ($n = 5$). (c) Immunohistochemistry images of STBD1, GRP78 and GAA in the heart tissues (bar: 100 μm, $N = 5$). (d) Western blot images of OPTN in the heart tissues ($n = 3$). (e) Western blot images of STBD1, GABARAPL1, GRP78, CHOP, and GAA in the heart tissues ($n = 3$). (f–k) Data were expressed as the expression ratio of OPTN/β-actin, STBD1/β-actin, GABARAPL1/β-actin, GRP78/β-actin, CHOP/β-actin, and GAA/β-actin. *$p < 0.05$, **$p < 0.01$ compared with control group (CCR and CCP); #$p < 0.05$, ##$p < 0.01$ compared with DMP group. CCR: control SAMR1 group; DMR: STZ-induced SAMR1 group; CCP: control SAMP8 group; DMP: STZ-induced SAMP8 group; DDP: DP-treated STZ-induced SAMP8 group. DP: D-pinitol; MFI: mean fluorescence intensity.

OsiRNA group had similar in protein expression of those ($p > 0.05$). These results suggest that glycophagy and ERS pathway are involved in OPTN-mediated H9C2 cell apoptosis in response to AGEs stimulation.
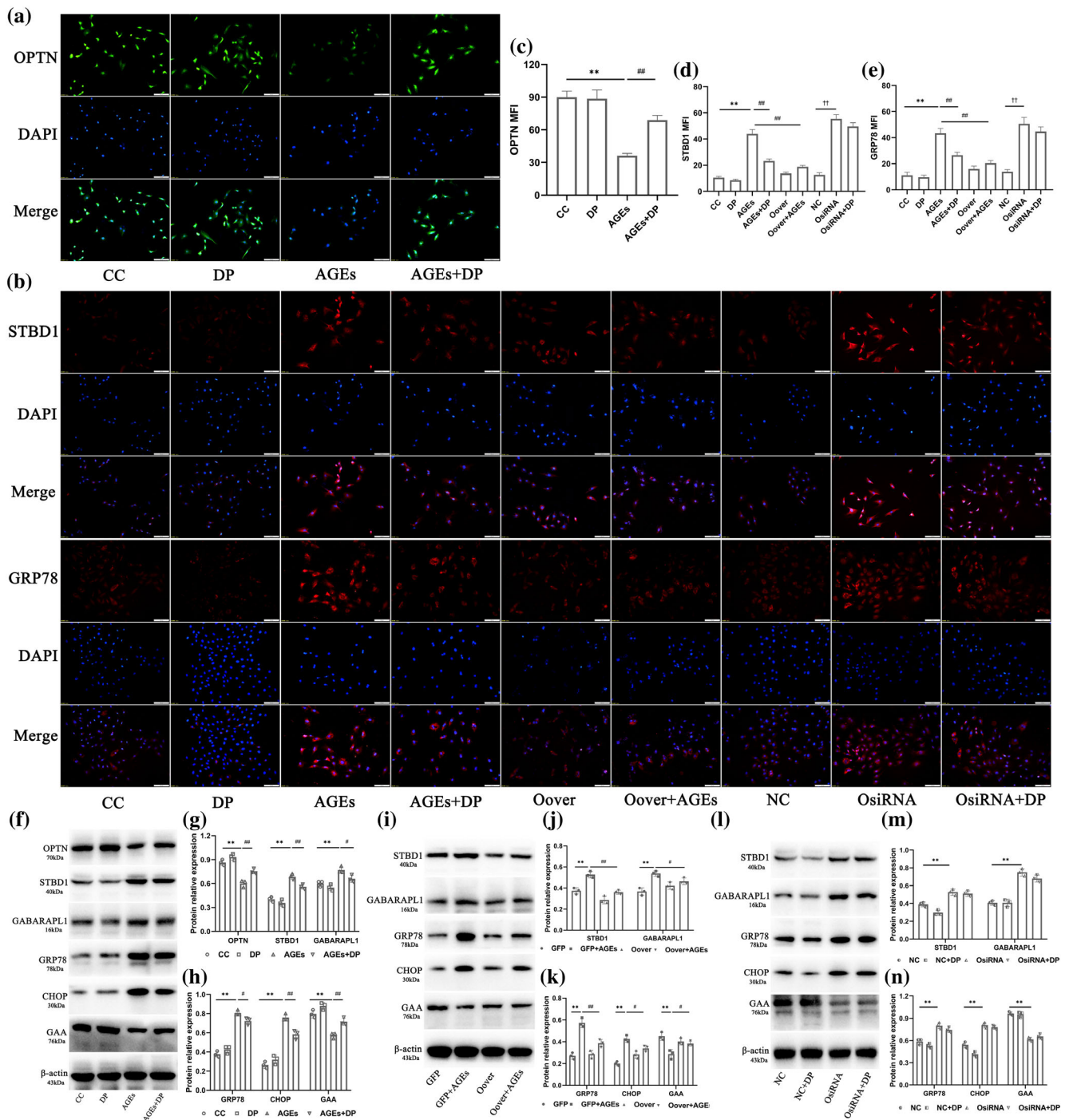
FIGURE 4 Effects of OPTN on STBD1, GABARAPL1, GRP78, CHOP, and GAA in H9C2 cells. (a) Immunofluorescent images of OPTN in H9C2 cells (bar: 100 μm, N = 3). (b) Immunofluorescent images of STBD1 and GRP78 in H9C2 cells (bar: 100 μm, N = 3). (c–e) MFI of OPTN, STBD1, and GRP78 in H9C2 cells (n = 3). (f) Western blot images of OPTN, STBD1, GABARAPL1, GRP78, CHOP, and GAA in AGEs-induced H9C2 cells (n = 3). (g, h) Data were expressed as the expression ratio of OPTN/β-actin, STBD1/β-actin, GABARAPL1/β-actin, GRP78/β-actin, CHOP/β-actin, and GAA/β-actin. (i) Western blot images of STBD1, GABARAPL1, GRP78, CHOP, and GAA in H9C2 cells with OPTN overexpression (n = 3). (j, k) Data were expressed as the expression ratio. (l) Western blot images of STBD1, GABARAPL1, GRP78, CHOP, and GAA in H9C2 cells with OPTN siRNA (n = 3). (m, n) Data were expressed as the expression ratio. $*p < 0.05$, $**p < 0.01$ compared with CC group; $^{\#}p < 0.05$, $^{\#\#}p < 0.01$ compared with AGEs group. $^{\dagger}p < 0.05$, $^{\dagger\dagger}p < 0.01$ compared with NC group; $^{\ddagger}p < 0.05$, $^{\ddagger\ddagger}p < 0.01$ compared with OsiRNA group. $*p < 0.05$, $**p < 0.01$ compared with GFP group; $^{\Diamond}p < 0.05$, $^{\Diamond\Diamond}p < 0.01$ compared with GFP + AGEs group. AGEs: advanced glycation end-products.
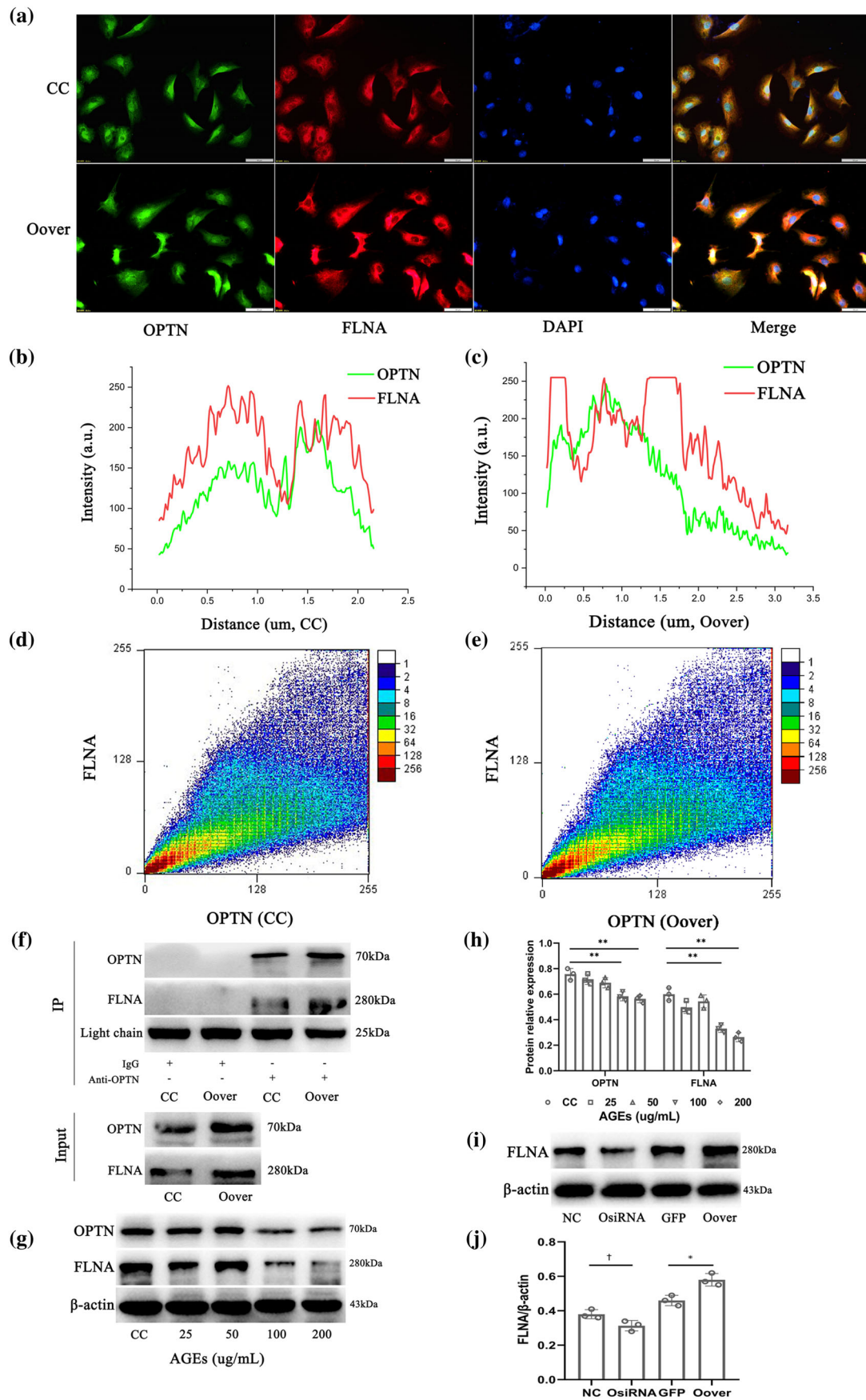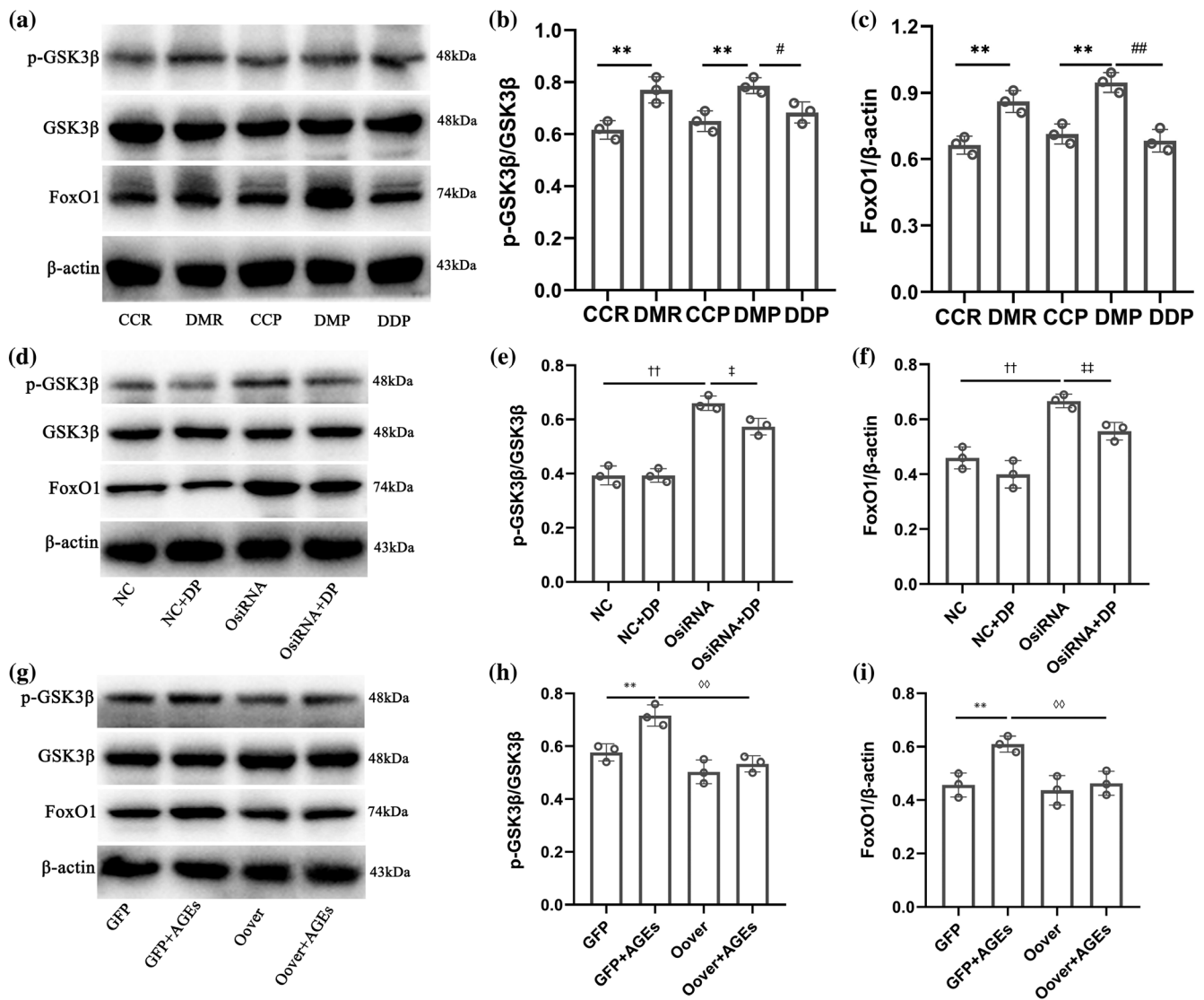
FIGURE 5 Legend on next page.

FIGURE 6 Effects of OPTN on phospho-GSK3β and FoxO1. (a) Western blot images of p-GSK3β, GSK3β, and FoxO1 in the heart tissues ($n = 3$). (b, c) Data were expressed as the expression ratio of p-GSK3β/GSK3β and FoxO1/β-actin. (d) Western blot images of p-GSK3β, GSK3β, and FoxO1 in H9C2 cells with OPTN siRNA ($n = 3$). (e, f) Data were expressed as the expression ratio of p-GSK3β/GSK3β and FoxO1/β-actin. (g) Western blot images of p-GSK3β, GSK3β, and FoxO1 in H9C2 cells with OPTN overexpression ($n = 3$). (h, i) Data were expressed as the expression ratio of p-GSK3β/GSK3β and FoxO1/β-actin. *$p < 0.05$, **$p < 0.01$ compared with control group (CCR and CCP); #$p < 0.05$, ##$p < 0.01$ compared with DMP group. †$p < 0.05$, ††$p < 0.01$ compared with NC group; ‡$p < 0.05$, ‡‡$p < 0.01$ compared with OsiRNA group. *$p < 0.05$, **$p < 0.01$ compared with GFP group; ◇$p < 0.05$, ◇◇$p < 0.01$ compared with GFP + AGEs group. CCR: control SAMR1 group; DMR: STZ-induced SAMR1 group; CCP: control SAMP8 group; DMP: STZ-induced SAMP8 group; DDP: DP-treated STZ-induced SAMP8 group.

FIGURE 5 Identification and confirmation of OPTN–FLNA interaction. (a) Immunofluorescence staining and co-localization analyses of OPTN (green) and FLNA (red) (bar: 50 μm, $N = 3$). (b–e) The overlap analysis of OPTN and FLNA in CC group and Oover group. (f) Western blot images of confirmation of OPTN-FLNA interaction in the immunoprecipitates ($n = 3$). (g) Western blot images of OPTN and FLNA in the different concentrations AGEs-induced H9C2 cells ($n = 3$). (h) Data were expressed as the expression ratio of OPTN/β-actin and FLNA/β-actin. (i) Western blot images of FLNA in H9C2 cells with OPTN siRNA and overexpression ($n = 3$). (j) Data were expressed as the expression ratio of FLNA/β-actin. *$p < 0.05$, **$p < 0.01$ compared with CC group. †$p < 0.05$, ††$p < 0.01$ compared with NC group. *$p < 0.05$, **$p < 0.01$ compared with GFP group.

3.7 | Identification and confirmation of OPTN–FLNA interaction

We obtained 147 interaction proteins of OPTN (score >40) by LC–MS/MS analysis. FLNA protein has a higher score (323.31) and sequence coverage (33.60), and was expected to be an essential interacting protein of OPTN (Supplementary Table S1, Figure S5). The relationship between OPTN and FLNA was performed by immunofluorescence. OPTN (green) and FLNA (red) coexisted in the cytoplasm in the CC group and Oover group (Figure 5a). The correlation coefficients were 0.77 and 0.87 in the CC group and Oover group, respectively (Figure 5b–e). By CO-IP and western blot assay, FLNA protein was detected in the beads incubated with OPTN antibody and not detected in the beads incubated with IgG antibody (Figure 5f). Moreover, AGEs inhibited the protein expression of OPTN and FLNA in a concentration-dependent manner (Figure 5g,h). The protein expression of FLNA significantly decreased in OsiRNA group compared with those in NC group ($p < 0.05$), whereas OPTN overexpression significantly increased the protein expression of FLNA compared with GFP group (Figure 5i,j, $p < 0.05$).

3.8 | Effects of OPTN on Phospho-GSK3β and FoxO1

The protein expression of p-GSK3β and FoxO1 was significantly increased in the heart tissues of diabetic groups (DMR and DMP), while DP significantly inhibited the protein expression of p-GSK3β and FoxO1 in the DDP group (Figure 6a–c, $p < 0.05$). Moreover, OPTN siRNA significantly increased the protein expression of p-GSK3β and FoxO1 ($p < 0.01$), while DP (80 μmol/L) inhibited the protein expression of p-GSK3β and FoxO1 for 48 h (Figure 6d–f, $p < 0.05$). Induction of GFP group with AGEs (200 μg/mL) resulted in a significant increase in the protein expression of p-GSK3β and FoxO1, whereas OPTN overexpression significantly attenuated AGEs induced the protein expression of p-GSK3β and FoxO1 for 48 h (Figure 6g–i, $p < 0.01$). These results suggest that OPTN regulated the ERS and glycophagy through GSK3β phosphorylation and FoxO1 signaling pathways.

4 | DISCUSSION

DCM is one of the main causes of heart failure in diabetic patients (Li et al., 2023; Wang et al., 2020). However, the mechanisms by which high circulating AGE levels cause DCM to remain poorly understood. In the present study, STZ-induced SAMR1 and SAMP8 mice were found to exhibit high serum and cardiac AGEs, cardiac dysfunction, ERS, glycophagy, myocardial apoptosis, and fibrosis compared with non-diabetic mice. Moreover, AGE stimulation significantly increased OPTN-mediated cardiomyocytes ERS, glycophagy, and apoptosis, whereas DP could significantly improve all of these changes in vivo and in vitro. These findings provide new insights into the pathogenesis of DCM and new theoretical evidence for the application of DP in the prevention and treatment of DCM.

Many studies showed that ERS caused by AGEs played a key role in diabetes and its complications (Du et al., 2023; Fernández et al., 2015; He et al., 2018). Excessive AGEs exacerbated coronary microvascular dysfunctions by activating ERS-mediated signaling pathway in diabetes. ERS could lead to the accumulation of unfolded proteins, contributing to myocardial apoptosis in diabetic animal models (Liu et al., 2021; Wu, Lu, et al., 2023; Wu, Xu, et al., 2023). The current study identified a novel physiological role of OPTN in reversing ERS-induced DCM. Diabetic mice exhibited obvious systolic dysfunction, diastolic dysfunction, and myocardial fibrosis, and OPTN expression decreased at 23 weeks. DP significantly increased the expression of OPTN and alleviated ERS and DCM.

It has been shown that ERS activation leads to the activation of numerous pathways in the pathophysiological processes of DCM. The interaction of ERS and glycophagy promotes cardiomyocyte apoptosis and necrosis. ERS can promote the accumulation of glycogen at endoplasmic reticulum sites. STBD1 is a glycogen-binding protein resident in the endoplasmic reticulum. STBD1 was identified as the downstream target of ERS response in C2C12 cells, specifically promoting the formation of endoplasmic reticulum-related glycogen clusters and responding to ERS activation (Kyriakoudi et al., 2022; Lytridou et al., 2020). Moreover, STBD1 is considered a selective autophagic receptor for glycogen and an important glycophagy medium. Some research suggests that the upregulation of glycophagy in DCM has opened up a new research field. Glycophagy disorder may play role in a mediating glycogen accumulation in DCM (Delbridge et al., 2015). Our study proved that cardiac glycogen content and glycophagy were significantly higher in diabetic mice. OPTN overexpression could inhibit the expression of STBD1 in the AGEs-induced H9C2 cells. Thus, OPTN is a crucial factor in AGEs-induced cardiomyocyte glycophagy and DCM.

Many studies have shown that OPTN is involved in the autophagy process, including cargo identification, autophagosome formation, autophagosome maturation, lysosomal quality control, and autophagic degradation (Qiu et al., 2022). OPTN is highly expressed in many tissues, including of heart, brain, and liver. OPTN-mediated autophagy dysfunction is closely related to amyotrophic lateral sclerosis, Parkinson disease, osteoporosis, acute kidney injury, and diabetic nephropathy. During the progression of diabetic nephropathy, the expression of OPTN is negatively correlated with renal function (Chen et al., 2018). It suggests that OPTN may play a renal protective role in high glucose-induced renal tubular epithelial cell senescence and diabetic nephropathy. Moreover, it regulates the signaling pathway induced by ERS and provides the protection against ERS-induced cell death (Ramachandran et al., 2021). In the present study, we found that OPTN had the cardioprotective effect in AGEs-induced H9C2 cells and DCM by regulating ERS and glycophagy.

However, we also discovered that FLNA is an important interacting protein of OPTN in the cardiomyocyte, which contributes to further analyzing the biological effects of OPTN. FLNA is an actin-binding protein that participates in the formation of cytoskeleton, cell
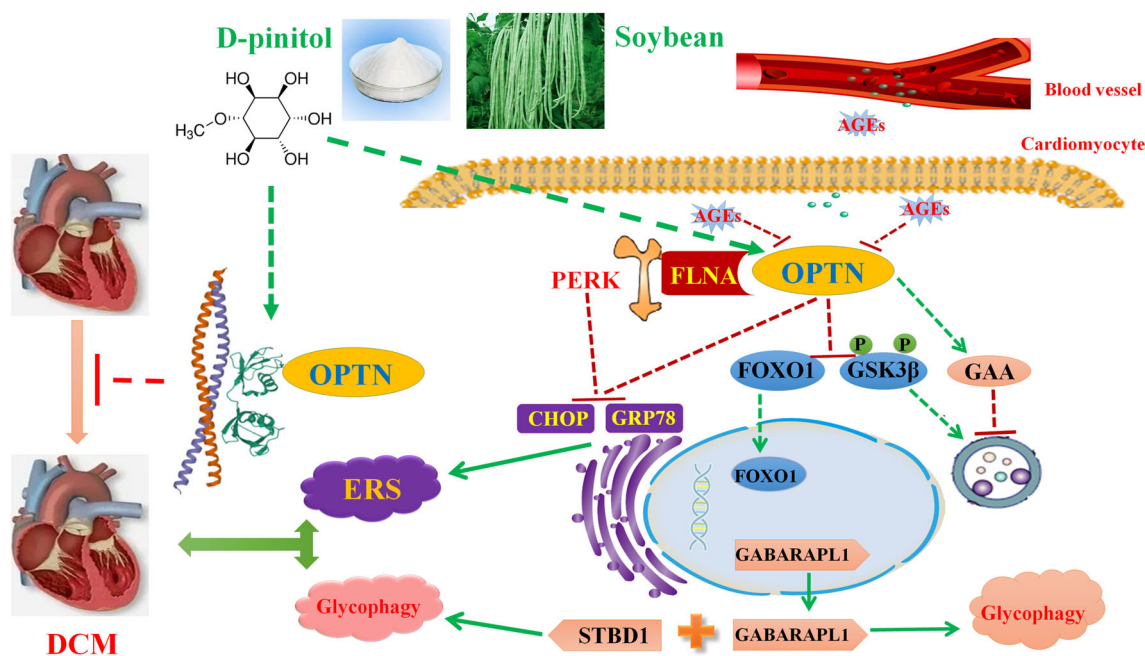
FIGURE 7 The diagram of OPTN-mediated ERS and glycophagy-induced signaling pathways in DCM and effects of DP. ERS: endoplasmic reticulum stress; DCM: diabetic cardiomyopathy; DP: D-pinitol.

proliferation and differentiation, and signal transduction (Métais et al., 2018; Zhou et al., 2021). Bandaru et al. reported that endothelial FLNA deficiency exacerbated left ventricular dysfunction and developed severe cardiac failure after myocardial infarction. FLNA provided a favorable method for inhibiting abnormal cardiac remodeling (Bandaru et al., 2015; Bandaru et al., 2021). FLNA is an important interacting protein of protein kinase RNA-like ER kinase (PERK). The interaction between FLNA and PERK regulated F-actin remodeling. It has been reported that AGEs can increase ERS via GRP78 and PERK/CHOP pathways (Belali et al., 2022). FLNA operates as an interphase between unfolded protein response and actin cytoskeleton and maintains endoplasmic reticulum proteostasis (van Vliet et al., 2017). We found out that OPTN overexpression significantly upregulated the expression FLNA, which was associated with the inhibition of ERS in DCM. Moreover, GSK3β and FoxO1 participate in the occurrence and development of DCM through ERS and glycophagy (Divari et al., 2020; Du et al., 2022; Wu, Lu, et al., 2023; Wu, Xu, et al., 2023). The beneficial effect of OPTN on DCM is likely through regulation of the GSK3β/FoxO1 pathway.

At present, it has been reported that DP could control postprandial blood glucose and improve the insulin resistance in patients with type 2 diabetes (Kang et al., 2006; Kim et al., 2012). The dose is 1.2 g/day in the patients with type 2 diabetes mellitus. The daily dosage of mice of DP is 150 mg/kg based on the body surface area conversion index of humans and mice. Moreover, swiss albino mice tolerated DP dose of up to 2 g/kg body weight and showed no toxic symptoms and any mortality (Chauhan et al., 2011). In our study, we found that DP (150 mg/kg) may be helpful to treat the onset of DCM. Targeting OPTN with DP could be translated into clinical application in the fighting against DCM.

5 | CONCLUSIONS

In summary, our findings suggested that DP reduced the blood glucose and AGEs, and increased the expression of heart OPTN in diabetic mice, thereby inhibiting the ERS and glycophagy, and alleviating the myocardial apoptosis and fibrosis of DCM. Moreover, OPTN could attenuate AGEs-induced ERS and glycophagy in vivo and in vitro. FLNA interacted with OPTN was downregulated by AGEs and further reduced the inhibitory effect of OPTN on ERS and glycophagy (Figure 7). Furthermore, our findings also provide insight into the potential role of OPTN in DCM via GSK3β phosphorylation and FoxO1 inhibition. This might be a new treatment strategy for patients with DCM, consistent with our enrichment analysis of DP targets.

AUTHOR CONTRIBUTIONS

Xiaoli Li: Conceptualization; formal analysis; funding acquisition; methodology; validation; writing – original draft. **Xin Yu:** Formal analysis; methodology; validation; writing – original draft. **Fei Yu:** Formal analysis; methodology; writing – review and editing. **Chunli Fu:** Formal analysis; methodology; validation. **Wenqian Zhao:** Formal analysis; methodology. **Xiaosong Liu:** Methodology; validation. **Chaochao Dai:** Methodology. **Haiqing Gao:** Project administration; writing – review and editing. **Mei Cheng:** Formal analysis; methodology; project administration; writing – review and editing. **Baoying Li:** Formal analysis; methodology; project administration; validation; writing – review and editing.

CONFLICT OF INTEREST STATEMENT

The authors declare that they have no competing interests.

DATA AVAILABILITY STATEMENT

The data that supports the findings of this study are available in the supplementary material of this article.

ORCID

Baoying Li https://orcid.org/0000-0002-5845-0720

REFERENCES

Ali, D. M., Ansari, S. S., Zepp, M., Knapp-Mohammady, M., & Berger, M. R. (2019). Optineurin downregulation induces endoplasmic reticulum stress, chaperone-mediated autophagy, and apoptosis in pancreatic cancer cells. *Cell Death Discovery*, *5*, 128. https://doi.org/10.1038/s41420-019-0206-2

Bandaru, S., Ala, C., Zhou, A. X., & Akyürek, L. M. (2021). Filamin A Regulates Cardiovascular Remodeling. *International Journal of Molecular Sciences*, *22*, 6555. https://doi.org/10.3390/ijms22126555

Bandaru, S., Grönros, J., Redfors, B., Çil, Ç., Pazooki, D., Salimi, R., Larsson, E., Zhou, A. X., Ömerovic, E., & Akyürek, L. M. (2015). Deficiency of filamin A in endothelial cells impairs left ventricular remodelling after myocardial infarction. *Cardiovascular Research*, *105*, 151–159. https://doi.org/10.1093/cvr/cvu226

Belali, O. M., Ahmed, M. M., Mohany, M., Belali, T. M., Alotaibi, M. M., Al-Hoshani, A., & Al-Rejaie, S. S. (2022). LCZ696 protects against diabetic cardiomyopathy-induced myocardial inflammation, ER stress, and apoptosis through inhibiting AGEs/NF-κB and PERK/CHOP signaling pathways. *International Journal of Molecular Sciences*, *23*, 1288. https://doi.org/10.3390/ijms23031288

Chauhan, P. S., Gupta, K. K., & Bani, S. (2011). The immunosuppressive effects of Agyrolobium roseum and pinitol in experimental animals. *International Immunopharmacology*, *11*, 286–291. https://doi.org/10.1016/j.intimp.2010.11.028

Chen, K., Dai, H., Yuan, J., Chen, J., Lin, L., Zhang, W., Wang, L., Zhang, J., Li, K., & He, Y. (2018). Optineurin-mediated mitophagy protects renal tubular epithelial cells against accelerated senescence in diabetic nephropathy. *Cell Death & Disease*, *9*, 105. https://doi.org/10.1038/s41419-017-0127-z

Chen, K., Feng, L., Hu, W., Chen, J., Wang, X., Wang, L., & He, Y. (2019). Optineurin inhibits NLRP3 inflammasome activation by enhancing mitophagy of renal tubular cells in diabetic nephropathy. *FASEB Journal*, *33*, 4571–4585. https://doi.org/10.1096/fj.201801749RRR

Delbridge, L. M., Mellor, K. M., Taylor, D. J., & Gottlieb, R. A. (2015). Myocardial autophagic energy stress responses—macroautophagy, mitophagy, and glycophagy. *American journal of physiology. Heart and Circulatory Physiology*, *308*, H1194–H1204. https://doi.org/10.1152/ajpheart.00002.2015

Divari, S., de Lucia, F., Berio, E., Sereno, A., Biolatti, B., & Cannizzo, F. T. (2020). Dexamethasone and prednisolone treatment in beef cattle: Influence on glycogen deposition and gene expression in the liver. *Domestic Animal Endocrinology*, *72*, 106444. https://doi.org/10.1016/j.domaniend.2020.106444

Du, H., Ma, Y., Wang, X., Zhang, Y., Zhu, L., Shi, S., Pan, S., & Liu, Z. (2023). Advanced glycation end products induce skeletal muscle atrophy and insulin resistance via activating ROS-mediated ER stress PERK/-FOXO1 signaling. *American journal of physiology Endocrinology and Metabolism*, *324*, E279–E287. https://doi.org/10.1152/ajpendo.00218.2022

Du, Z., Hu, J., Lin, L., Liang, Q., Sun, M., Sun, Z., & Duan, J. (2022). Melatonin alleviates PM2.5 -induced glucose metabolism disorder and lipidome alteration by regulating endoplasmic reticulum stress. *Journal of Pineal Research*, *73*, e12823. https://doi.org/10.1111/jpi.12823

Fernández, A., Ordóñez, R., Reiter, R. J., González-Gallego, J., & Mauriz, J. L. (2015). Melatonin and endoplasmic reticulum stress: Relation to autophagy and apoptosis. *Journal of Pineal Research*, *59*, 292–307. https://doi.org/10.1111/jpi.12264

He, Y., Zhou, L., Fan, Z., Liu, S., & Fang, W. (2018). Palmitic acid, but not high-glucose, induced myocardial apoptosis is alleviated by N-acetylcysteine due to attenuated mitochondrial-derived ROS accumulation-induced endoplasmic reticulum stress. *Cell Death & Disease*, *9*, 568. https://doi.org/10.1038/s41419-018-0593-y

Hu, X., Wong, S. W., Liang, K., Wu, T. H., Wang, S., Wang, L., Liu, J., Yamauchi, M., Foster, B. L., Ting, J. P., Zhao, B., Tseng, H. C., & Ko, C. C. (2023). Optineurin regulates NRF2-mediated antioxidant response in a mouse model of Paget's disease of bone. *Science Advances*, *9*, eade6998. https://doi.org/10.1126/sciadv.ade6998

Jia, G., DeMarco, V. G., & Sowers, J. R. (2016). Insulin resistance and hyperinsulinaemia in diabetic cardiomyopathy. *Nature Reviews. Endocrinology*, *12*, 144–153. https://doi.org/10.1038/nrendo.2015.216

Jia, G., Whaley-Connell, A., & Sowers, J. R. (2018). Diabetic cardiomyopathy: A hyperglycaemia- and insulin-resistance-induced heart disease. *Diabetologia*, *61*, 21–28. https://doi.org/10.1007/s00125-017-4390-4

Kang, M. J., Kim, J. I., Yoon, S. Y., Kim, J. C., & Cha, I. J. (2006). Pinitol from soybeans reduces postprandial blood glucose in patients with type 2 diabetes mellitus. *Journal of Medicinal Food*, *9*, 182–186. https://doi.org/10.1089/jmf.2006.9.182

Kim, H. J., Park, K. S., Lee, S. K., Min, K. W., Han, K. A., Kim, Y. K., & Ku, B. J. (2012). Effects of pinitol on glycemic control, insulin resistance and adipocytokine levels in patients with type 2 diabetes mellitus. *Annals of Nutrition & Metabolism*, *60*, 1–5. https://doi.org/10.1159/000334834

Koutsifeli, P., Varma, U., Daniels, L. J., Annandale, M., Li, X., Neale, J. P. H., Hayes, S., Weeks, K. L., James, S., Delbridge, L. M. D., & Mellor, K. M. (2022). Glycogen-autophagy: Molecular machinery and cellular mechanisms of glycophagy. *The Journal of Biological Chemistry*, *298*, 102093. https://doi.org/10.1016/j.jbc.2022.102093

Kyriakoudi, S., Theodoulou, A., Potamiti, L., Schumacher, F., Zachariou, M., Papacharalambous, R., Kleuser, B., Panayiotidis, M. I., Drousiotou, A., & Petrou, P. P. (2022). Stbd1-deficient mice display insulin resistance associated with enhanced hepatic ER-mitochondria contact. *Biochimie*, *200*, 172–183. https://doi.org/10.1016/j.biochi.2022.06.003

Li, X., Li, Z., Dong, X., Wu, Y., Li, B., Kuang, B., Chen, G., & Zhang, L. (2023). Astragaloside IV attenuates myocardial dysfunction in diabetic cardiomyopathy rats through downregulation of CD36-mediated ferroptosis. *Phytotherapy Research*, *37*, 3042–3056. https://doi.org/10.1002/ptr.7798

Li, X., Zhang, D. Q., Wang, X., Zhang, Q., Qian, L., Song, R., Zhao, X., & Li, X. (2022). Irisin alleviates high glucose-induced hypertrophy in H9c2 cardiomyoblasts by inhibiting endoplasmic reticulum stress. *Peptides*, *152*, 170774. https://doi.org/10.1016/j.peptides.2022.170774

Li, X. L., Xu, M., Yu, F., Fu, C. L., Yu, X., Cheng, M., & Gao, H. Q. (2021). Effects of D-pinitol on myocardial apoptosis and fibrosis in streptozocin-induced aging-accelerated mice. *Journal of Food Biochemistry*, *45*(4), e13669. https://doi.org/10.1111/jfbc.13669

Li, X. L., Yu, F., Fu, C. L., Yu, X., Xu, M., & Cheng, M. (2022). Phosphoproteomics analysis of diabetic cardiomyopathy in aging-accelerated mice and effects of D-pinitol. *Proteomics. Clinical Applications*, *16*(1), e2100019. https://doi.org/10.1002/prca.202100019

Liu, F., Ye, F., Cheng, C., Kang, Z., Kou, H., & Sun, J. (2022). Symbiotic microbes aid host adaptation by metabolizing a deterrent host pine

carbohydrate d-pinitol in a beetle-fungus invasive complex. *Science Advances*, *8*, eadd5051. https://doi.org/10.1126/sciadv.add5051

Liu, Z., Zhu, H., Ma, Y., Tang, Z., Zhao, N., Wang, Y., & Pan, S. (2021). AGEs exacerbates coronary microvascular dysfunction in NoCAD by activating endoplasmic reticulum stress-mediated PERK signaling pathway. *Metabolism: Clinical and Experimental*, *117*, 154710. https://doi.org/10.1016/j.metabol.2021.154710

Lytridou, A. A., Demetriadou, A., Christou, M., Potamiti, L., Mastroyiannopoulos, N. P., Kyriacou, K., Phylactou, L. A., Drousiotou, A., & Petrou, P. P. (2020). Stbd1 promotes glycogen clustering during endoplasmic reticulum stress and supports survival of mouse myoblasts. *Journal of Cell Science*, *133*, jcs244855. https://doi.org/10.1242/jcs.244855

Métais, A., Lamsoul, I., Melet, A., Uttenweiler-Joseph, S., Poincloux, R., Stefanovic, S., Valière, A., Gonzalez de Peredo, A., Stella, A., Burlet-Schiltz, O., Zaffran, S., Lutz, P. G., & Moog-Lutz, C. (2018). Asb2α-filamin A axis Is essential for actin cytoskeleton remodeling during heart development. *Circulation Research*, *122*, e34–e48. https://doi.org/10.1161/CIRCRESAHA.117.312015

Mandl, J., & Bánhegyi, G. (2018). The ER–glycogen particle–phagophore triangle: A hub connecting glycogenolysis and Glycophagy? *Pathology Oncology Research*, *24*, 821–826. https://doi.org/10.1007/s12253-018-0446-0

Medina-Vera, D., Navarro, J. A., Rivera, P., Rosell-Valle, C., Gutiérrez-Adán, A., Sanjuan, C., López-Gambero, A. J., Tovar, R., Suárez, J., Pavón, F. J., Baixeras, E., Decara, J., & Rodríguez de Fonseca, F. (2022). d-Pinitol promotes tau dephosphorylation through a cyclin-dependent kinase 5 regulation mechanism: A new potential approach for tauopathies? *British Journal of Pharmacology*, *179*, 4655–4672. https://doi.org/10.1111/bph.15907

Mellor, K. M., Varma, U., Stapleton, D. I., & Delbridge, L. M. (2014). Cardiomyocyte glycophagy is regulated by insulin and exposure to high extracellular glucose. *American Journal of Physiology-Heart and Circulatory Physiology*, *306*, H1240–H1245. https://doi.org/10.1152/ajpheart.00059.2014

Preetha Rani, M. R., Salin Raj, P., Nair, A., Ranjith, S., Rajankutty, K., & Raghu, K. G. (2022). In vitro and in vivo studies reveal the beneficial effects of chlorogenic acid against ER stress mediated ER-phagy and associated apoptosis in the heart of diabetic rat. *Chemico-Biological Interactions*, *351*, 109755. https://doi.org/10.1016/j.cbi.2021.109755

Qiu, Y., Wang, J., Li, H., Yang, B., Wang, J., He, Q., & Weng, Q. (2022). Emerging views of OPTN (optineurin) function in the autophagic process associated with disease. *Autophagy*, *18*, 73–85. https://doi.org/10.1080/15548627.2021.1908722

Ramachandran, G., Moharir, S. C., Raghunand, T. R., & Swarup, G. (2021). Optineurin modulates ER stress-induced signaling pathways and cell death. *Biochemical and Biophysical Research Communications*, *534*, 297–302. https://doi.org/10.1016/j.bbrc.2020.11.091

van Vliet, A. R., Giordano, F., Gerlo, S., Segura, I., Van Eygen, S., Molenberghs, G., Rocha, S., Houcine, A., Derua, R., Verfaillie, T., Vangindertael, J., De Keersmaecker, H., Waelkens, E., Tavernier, J., Hofkens, J., Annaert, W., Carmeliet, P., Samali, A., Mizuno, H., & Agostinis, P. (2017). The ER stress sensor perk coordinates ER-plasma membrane contact site formation through interaction with Filamin-A and F-actin remodeling. *Molecular Cell*, *65*, 885–899.e6. https://doi.org/10.1016/j.molcel.2017.01.020

Wang, Y., Luo, W., Han, J., Khan, Z. A., Fang, Q., Jin, Y., Chen, X., Zhang, Y., Wang, M., Qian, J., Huang, W., Lum, H., Wu, G., & Liang, G. (2020). MD2 activation by direct AGE interaction drives inflammatory diabetic cardiomyopathy. *Nature Communications*, *11*, 2148. https://doi.org/10.1038/s41467-020-15978-3

Wu, L. X., Xu, Y. C., Pantopoulos, K., Tan, X. Y., Wei, X. L., Zheng, H., & Luo, Z. (2023). Glycophagy mediated glucose-induced changes of hepatic glycogen metabolism via OGT1-AKT1-FOXO1Ser238 pathway. *The Journal of Nutritional Biochemistry*, *117*, 109337. https://doi.org/10.1016/j.jnutbio.2023.109337

Wu, S., Lu, D., Gajendran, B., Hu, Q., Zhang, J., Wang, S., Han, M., Xu, Y., & Shen, X. (2023). Tanshinone IIA ameliorates experimental diabetic cardiomyopathy by inhibiting endoplasmic reticulum stress in cardiomyocytes via SIRT1. *Phytotherapy Research*, *37*, 3543–3558. https://doi.org/10.1002/ptr.7831

Zhao, H., Tang, M., Liu, M., & Chen, L. (2018). Glycophagy: An emerging target in pathology. *Clinica Chimica Acta; International Journal of Clinical Chemistry*, *484*, 298–303. https://doi.org/10.1016/j.cca.2018.06.014

Zhou, J., Kang, X., An, H., Lv, Y., & Liu, X. (2021). The function and pathogenic mechanism of filamin a. *Gene*, *784*, 145575. https://doi.org/10.1016/j.gene.2021.145575

SUPPORTING INFORMATION

Additional supporting information can be found online in the Supporting Information section at the end of this article.